The Astronomical Journal, 164:161 (7pp), 2022 October https://doi.org/10.3847/1538-3881/ac898b

Tying Spitzer's IRS Calibration to IRAC: Observations of IRS Standard Stars

Kathleen E. Kraemer[1], Charles W. Engelke[1], Bailey A. Renger[1], and G. C. Sloan[2,3]
[1] Institute for Scientific Research, Boston College, 140 Commonwealth Avenue, Chestnut Hill, MA 02467, USA; kathleen.kraemer@bc.edu
[2] Space Telescope Science Institute, 3700 San Martin Drive, Baltimore, MD 21218, USA
[3] Department of Physics and Astronomy, University of North Carolina, Chapel Hill, NC 27599-3255, USA
Received 2021 October 27; revised 2022 August 11; accepted 2022 August 11; published 2022 September 27

Abstract

We present 3.6 and 4.5 μm photometry for a set of 61 standard stars observed by Spitzer's Infrared Spectrograph (IRS). The photometry was obtained with the Infrared Array Camera (IRAC) on Spitzer in order to help tie the calibration of IRAC and the IRS, which had been anchored to the calibration of the Multiband Infrared Photometer for Spitzer. The wavelength range of the IRS data only slightly overlaps with the IRAC 4.5 μm band and not at all with the 3.6 μm band. Therefore, we generated synthetic spectra from spectral templates of stars with the same spectral types and luminosity classes as our sample stars, normalized to the IRS data at 6–7 μm, and compared those to the observed photometry. The new IRAC observations of IRS standard stars demonstrate that the two instruments are calibrated to within 1% of each other.

Unified Astronomy Thesaurus concepts: Infrared photometry (792); Photometric standard stars (1232); Flux calibration (544); Spectrophotometry (1556); Spectrophotometric standards (1555)

Supporting material: machine-readable tables

1. Introduction

The calibration of the Infrared Spectrograph (IRS; Houck et al. 2004) on the Spitzer Space Telescope is based on numerous observations of spectrophotometric standard stars, combined with model atmospheres (Sloan et al. 2015). The two primary standards were the A dwarfs α Lac and δ UMi, and the calibration was then transferred to the rest of the A-dwarf and K-giant sample. The absolute flux calibration was pinned at the red end of the spectrum to the 24 μm calibration of the Multiband Imaging Photometer for Spitzer (MIPS; Rieke et al. 2004, 2008) using 22 μm photometry from the IRS Red Peak-Up array. Sloan & Ludovici (2012) estimated that the uncertainty in the spectroscopic calibration–that is, the point-to-point flux densities of the spectra–is better than 1%.

However, this estimate does not include the uncertainty in the absolute flux calibration of the IRS. In particular, the short-wavelength end of the spectra was never formally compared to photometric measurements during the cryogenic mission. Ideally, the calibration stars would have been observed with the Infrared Array Camera (IRAC; Fazio et al. 2004) I3 and I4 bands at 5.8 and 8.0 μm concurrently with IRS observations, as those bands overlapped with the IRS spectral coverage (Figure 1). This would have provided the most straightforward cross-calibration between the two instruments, and could have helped verify the 1.5% difference between MIPS and IRAC reported by Rieke et al. (2008).

Since such standards were not observedduring the cryogenic phase, we obtained Warm Spitzer observations in the 3.6 and 4.5 μm bands (I1 and I2). Section 2 describes the observations and data processing. We compare the measured photometry to synthetic photometry from stellar templates for each star in Sections 3, and 4 summarizes our findings.

2. Observations and Data Reduction

2.1. Source Selection and IRS Data

The IRS instrument team observed several dozen calibration sources over the course of the mission, primarily K giants and A dwarfs, along with bright stars and very red sources such as galaxies. We selected the set of K giants and A dwarfs described by Sloan et al. (2015). We also included several fainter K giants and solar analogs that were added to the calibration list later in the mission. Our sample contained 61 stars: 20 A dwarfs, 3 G dwarfs (solar analogs), and 38 K giants. To simplify the discussion, we include the one B9 dwarf and two late G giants in the A-dwarf and K-giant categories, respectively. Tables 1 and 2 list the observed sample, with the solar analogs included with the A dwarfs in Table 1.

For the IRS spectra of these sources, we use the spectral data reductions from Sloan et al. (2015), which readers should refer to for details on the IRS data processing. The spectral types listed in Tables 1 and 2 are also taken from Sloan et al. (2015), with two exceptions. We assign a spectral type of A1 V for HD 165459, following Reach et al. (2005). The spectral type for λ Tel is discussed in Section 2.6.

2.2. IRAC Observations

Each star was observed in subarray mode with the "Small 4-Position Gaussian" dither pattern to mitigate bad pixels and gain variations. The integration times ($t_{\rm int}$) were based on the flux densities (F_ν) estimated from the partially saturated measurements from the Wide-field Infrared Survey Experiment (WISE; Wright et al. 2010) in the AllWISE source catalog (Cutri et al. 2013).Although the saturation compromised the data for calibration use, they could still be used for estimating IRAC flux densities and setting integration times. These were $t_{\rm int} = 0.02$ s ($F_\nu > 3$ Jy), 0.1 s (0.7–3 Jy), or 0.4 s (<0.7 Jy), i.e., the longest time without saturating.Both bands used the same integration time to simplify the observational setup. With the chosen integration times and estimated flux densities, the

Table 1
Observations: A Dwarfs and Solar Analogs

Star Name	R.A. (J2000)	decl. (J2000)	Spectral Type	Observ. Date	AOR Key	t_{int} (s)
λ Tel	18 58 27.77	−52 56 19.1	B9 IV/V[a]	2015 Dec 16	58140160	0.02
…[b]	…	…	…	2016 Jun 27	58898176	0.02
η^1 Dor	06 06 09.38	−66 02 22.6	A0 V	2019 May 04	68758016	0.02
HD 46190	06 27 48.62	−62 08 59.7	A0 V	2016 Jan 20	58141184	0.10
ξ^1 Cen	13 03 33.31	−49 31 38.2	A0 V	2016 May 12	58139904	0.02

Notes. This table is available in its entirety in machine-readable format.
[a] See text regarding the luminosity class of λ Tel.
[b] Ellipses indicate λ Tel was one of the stars observed twice.

(This table is available in its entirety in machine-readable form.)

Table 2
Observations: K Giants

Star Name	R.A. (J2000)	decl. (J2000)	Spectral Type	Observ. Date	AOR Key	t_{int} (s)
BD+00 2862	11 56 54.19	−00 30 13.5	G8 III	2016 Mar 20	58130432	0.40
HR 6606	17 37 08.88	+72 27 20.9	G9 III	2019 Apr 01	68757504	0.02
HD 41371	06 00 07.71	−64 18 36.0	K0 III	2019 Apr 25	68756992	0.02
HD 51211	06 50 25.27	−69 59 10.5	K0 III	2015 Dec 18	58136576	0.02
…	…	…	…	2016 May 26	58898944	0.02

Note. This table is available in its entirety in machine-readable format.

(This table is available in its entirety in machine-readable form.)

expected signal-to-noise ratios were ∼100–200 in each band for all stars. Table 1 includes observing details for the A dwarfs and Table 2 gives those for the K giants.

Most of the observations were made under Program 12059 in 2015–2016, with 11 additional stars observed under Program 14221 in 2019. Thirteen stars were observed twice because the temperature of the 4.5 μm array was unstable due to an IRAC/Spacecraft Communications anomaly from 2015 November 27 to December 14, the time of the first observations (S. Carey 2016, private communication). As explained in Section 2.5, we include both observations for these stars. HD 165459, a calibration target for IRAC, was observed three times, once at each integration time. Our final sample contains 76 observations of the 61 stars.

2.3. Data Reduction

The processing pipeline started with the basic calibrated data (BCD) from the Spitzer archive, pipeline version 19.2.0. In the IRAC subarray mode, an observation consists of 64 frames, which are provided in the BCD fits file. Each BCD corresponds to one of the four dither positions, and each star was observed in both the I1 and I2 bands.

Aperture photometry was performed on each frame with the *sextractor* softwarewith a 6 pixel diameter for the aperture and a (local) background annulus of 8 pixels. To correct for photometric variations due to the location of the source on the array and within a pixel, we used the IRAC_APHOT_CORR.pro[4] created by J. Ingalls and provided by the Spitzer Science Center (SSC), using positions from the SSC's BOX_CENTROIDER procedure. These corrections to the intrapixel response can be up to a few percent, so they are important to take into account for this project. *Sextractor* positions are determined by a different method, though, and cannot be used directly with IRAC_APHOT_CORR.

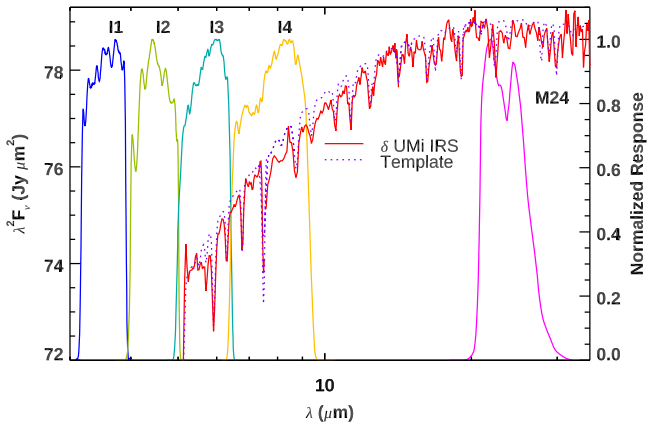

Figure 1. IRS spectrum of δ UMi (red line) compared to a scaled Kurucz model (purple dotted line). The spectra are shown in Rayleigh–Jeans (RJ) flux units, $\lambda^2 F_\nu$, in which the RJ tail of a blackbody would be a horizontal line. Also shown are the IRAC bands and the MIPS 24 μm band, each normalized to a peak of 1.

The aperture corrections were based on the values in the IRAC Handbook (v4.0), Table 4.2. The Handbook gives the conversion factors *zmag* and *C* to convert from surface brightness to flux density for 0.″6 pixels (appropriate for mosaics from, e.g., MOPEX), as opposed to the 1.″2 native pixels used here. For the larger pixels, the conversion factor becomes $C = 33.84638 \times 10^{-6}$ Jy/pixel/(MJy/sr) (cf., 8.461595×10^{-6} Jy/pixel/(MJy/sr) for the 0.″6 pixels) and $zmag = 17.297$ mag for I1 and 16.813 mag for I2.

[4] https://irsa.ipac.caltech.edu/data/SPITZER/docs/dataanalysistools/tools/contributed/.

Table 3
Observed Photometry

Star Name	AOR Key	$F_{3.6}$ (Jy)	$F_{4.5}$ (Jy)
λ Tel	58140160	3.078 ± 0.034	1.960 ± 0.003
⋯	58898176	3.070 ± 0.018	1.959 ± 0.011
η^1 Dor	68758016	1.405 ± 0.009	0.891 ± 0.007
HD 46190	58141184	0.799 ± 0.005	0.512 ± 0.004
ξ^1 Cen	58139904	3.586 ± 0.034	2.296 ± 0.018

Note. This table is available in its entirety in machine-readable format.

(This table is available in its entirety in machine-readable form.)

The photometry from the 64 frames was averaged into a single value for each dither position (i.e., each BCD). The standard deviation among the frames of a given position was $\sigma_f \sim 0.3\%$–2.3% and 0.4%–3.4% with means of 0.7% and 1.0% for I1 and I2, respectively. The variation among the four BCD s for a given star $\sigma_b \sim 0.2\%$–1.5% and 0.2%–2.0% with means of 0.8% for both I1 and I2.

2.4. Photometric Calibration with HD 165459

We used archival IRAC data of HD 165459, which was one of the primary IRAC calibration sources (e.g., Reach et al. 2005), to calibrate our observations and verify our processing pipeline. Reach et al. (2005) give the spectral type of HD 165459 as A1 V. They also give its brightness as $[3.6] = 6.593$ mag and $[4.5] = 6.575$ mag, which correspond to $F_{3.6} = 0.648$ Jy and $F_{4.5} = 0.421$ Jy. We use these values as the fiducial standard values in the following discussion.

We processed 22 IRAC calibration observations taken with the subarray between 30 Oct 2015 and 17 Sep 2016, which span the observation dates forPID 12059. These observations used the large-scale 4-position Gaussian dither pattern with $t_{\rm int} = 0.4$ s (the two calibration observations with the subarray at 0.02 or 0.1 s in this time frame were not dithered).

The result of processing these data finds that the flux densities from our pipeline were too faint compared to Reach et al. (2005) by $3.64\% \pm 0.21\%$ for I1 and $3.57\% \pm 0.27\%$ for I2. The uncertainties, σ_{cal}, are the standard deviations among the 88 measurements (four dither positions for each of the 22 observations). Additional details, including the photometry, are given in the Appendix.

Table 3 reports the resulting flux densities for our targets. These are the weighted means of the four BCD s (weighted by σ_f), adjusted in magnitude space by subtracting the magnitude offsets from the HD 165459 calibration data to correct the bias in our pipeline. This aligns our results with the photometric calibration of IRAC by Reach et al. (2005). The quoted uncertainties are from σ_b, the standard deviation of those four measurements, and σ_{cal}, the calibration bias uncertainty, added in quadrature.

2.5. Array Temperature Drift Effect

Thirteen stars were observed twice due to a concern by the SSC regarding a small drift in the temperature of the I2 focal plane array (FPA) from an IRAC/Spacecraft anomaly. The mean temperature of the array was $T_{4.5,\rm v1} = 27.873 \pm 0.018$ K for the first set (those taken before HMJD 57375) and $T_{4.5,\rm v2} = 28.687 \pm 0.003$ K for the second set; quoted uncertainties are 1σ standard deviations. For comparison, the temperatures at 3.6 μm were $T_{3.6} = 28.655 \pm 0.001$ K and 28.708 ± 0.002 K, respectively. Figure 2 shows the ratios of the first to second measurements $R\ (\rm v1/v2) = F_\nu\ (\rm v1)/F_\nu\ (\rm v2)$ as a function of the flux density from the first observation, $F_{3.6}$ (v1).

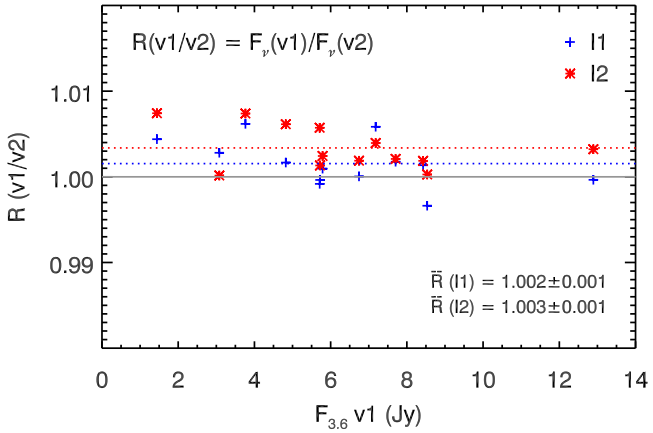

Figure 2. The ratios of the first and second measurements (v1 and v2, respectively) for I1 (blue pluses), and I2 (red asterisks) for the 13 stars with two observations. The flux density ratios are plotted versus $F_{3.6}$ v1. The blue dotted line shows the mean ratio for I1 and the red dotted line shows the mean ratio for I2.

The mean ratios are 1.002 ± 0.001 and 1.003 ± 0.001 for bands I1 and I2, respectively. That is, the second measurements are slightly lower than the first measurements, although the statistical significance is marginal. For individual stars, the difference between the two observations is always within the uncertainty of at least one measurement and most are them for both measurements (22 of the 26 data points). We conclude that the change in FPA temperature for I2 does not affect the measured photometry and therefore include both measurements in our analysis.

2.6. Spectral Templates

The IRS wavelength range did not significantly overlap with the I1 and I2 bands, so we cannot compare the IRAC photometry to the IRS spectra directly. To extend the spectra to shorter wavelengths and generate synthetic photometry, we instead use the stellar templating procedures pioneered by Cohen et al. (1992, 1995, 1999) and updated by Engelke et al. (2006). The templates for the K giants are derived from the stars of Engelke et al. (2006), which were based on the spectral library of Pickles (1998) and the spectral atlas of Sloan et al. (2003) from the Short-Wavelength Spectrometer (SWS; de Graauw et al. 1996) on the Infrared Space Observatory (Kessler et al. 1996). The templates for the A dwarfs are based on Kurucz atmospheric models.[5] The templates are interpolated in temperature space and angular diameter to fit the individual stars in our sample. The spectral type is used to set the initial temperatureand diameter, and a least-squares fit to visible and infrared photometry from the literature is performed.

Each template is normalized to the corresponding IRS data between 6 and 7 μm, i.e., between the molecular absorption bands dominated by CO at 5 μm and SiO starting at 7.5 μm in the K giants. This range was also used for the A dwarfs for consistency. Figure 3 shows the IRS data for a set of the most

[5] http://kurucz.harvard.edu/

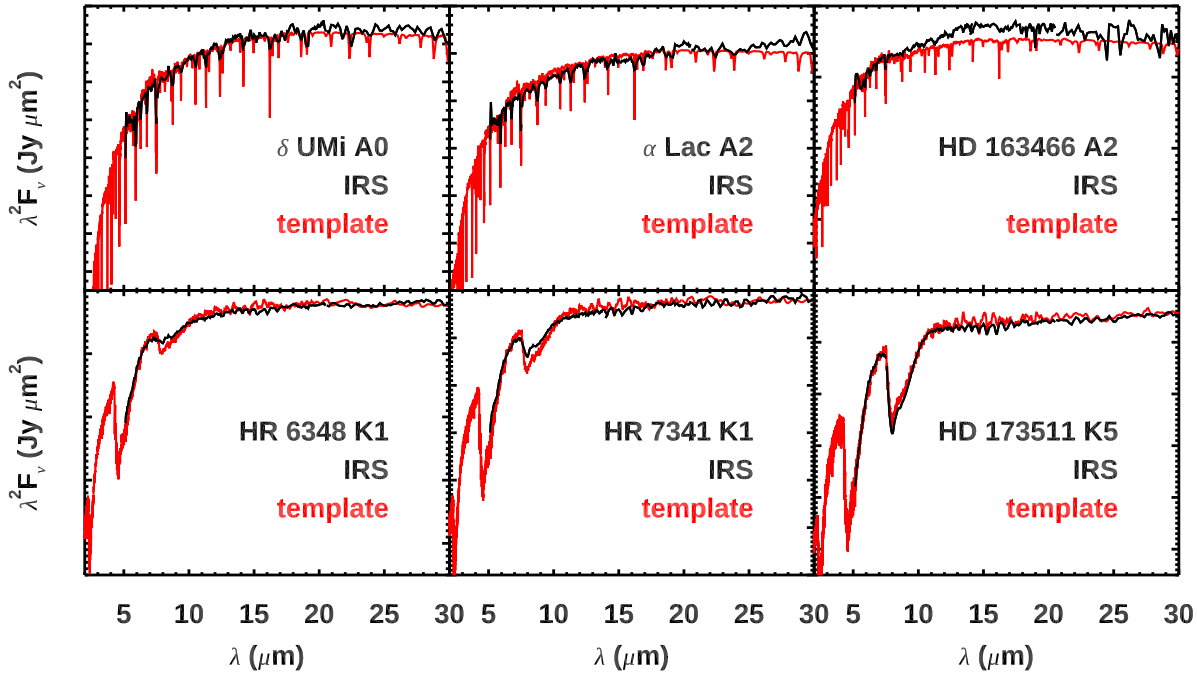

Figure 3. Comparison of IRS data and spectral templates for six of the IRS standards observed the most frequently, in RJ flux units. Templates (red) were normalized to the IRS data (black) between 6 and 7 μm.

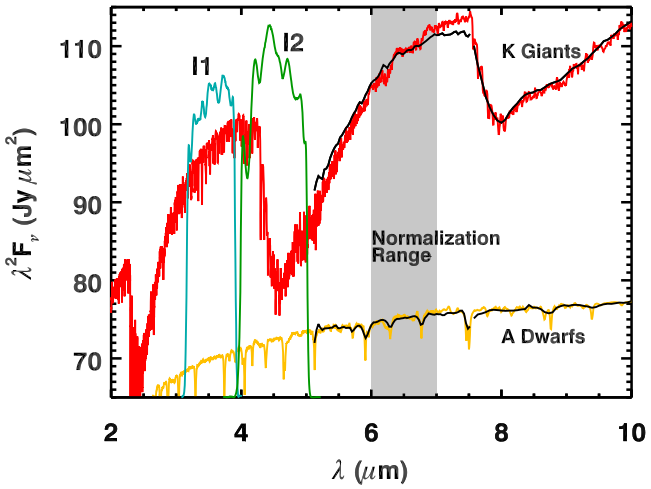

Figure 4. IRAC subarray RSRFswith representative spectra for a K giant and an A dwarf. Band I1 (3.6 μm) is in cyan and I2 (4.5 μm) in green. The black curves show measured IRS data for two stars in our sample, and the red and gold curves are the SWS-based templates. The templates were normalized to the IRS data at 6.0–7.0 μm (gray box).

frequently observed A dwarfs and K giants, which thus have high signal-to-noise ratios, along with the corresponding spectral templates used for the synthetic photometry.

Seven stars were not templated, although their IRAC photometry is included in the tables.HD 162317 has a very noisy IRS spectrum which precludes a reliable normalization for the template. λ Tel has an ambiguous spectral type suggesting that it is not a normal main-sequence star.[6] HD 196850, HD 176841, and HD 73350 are solar analogs, but the IRS spectra for two of them were too noisy to use. Also, we do not have a full set of validated templates for G dwarfs and did not have a good match for the third. HR 5949 and HD 46190 have excess emission from debris disks even at the shorter wavelengths (see, Sloan et al. 2015, their Figure 24).

Overall, we have 16 templated A dwarfs with 18 IRAC observations, and 37 templated K giants with 47 observations.

Table 4
Observed to Synthetic Ratios

Star Name	I1 $F_{3.6obs}$ (Jy)	I1 $F_{3.6syn}$ (Jy)	I1 Obs/Syn	I2 $F_{4.5obs}$ (Jy)	I2 $F_{4.5syn}$ (Jy)	I2 Obs/Syn
α Lac	8.986	8.955	1.004	5.807	5.743	1.011
δ UMi	5.650	5.622	1.005	3.637	3.605	1.009
ϵ Aqr	9.534	10.049	0.949	6.163	6.470	0.953
μ PsA	5.294	5.289	1.001	3.403	3.380	1.007
ν Tau v1	8.533	8.451	1.010	5.515	5.415	1.018
ν Tau v2	8.562	8.451	1.013	5.513	5.415	1.018

Note. This table is available in its entirety in machine-readable format. Labels "v1" and "v2" in the names refer to photometry from the first and second measurements for the 13 stars which were observed twice.

(This table is available in its entirety in machine-readable form.)

3. Results

We generated the synthetic photometry from the templates using the subarray-specific relative spectral response functions (RSRFs) for the warm mission obtained from the SSC website.[7] Figure 4 shows the RSRFs, two sample templates, and their IRS spectra, along with the normalization region. Table 4 gives the synthetic and observed flux densities and their ratio in the two bands for each star with a template.

[6] Sloan et al. (2015) report a spectral type of B9 III, based on de Vaucouleurs (1957) and Buscombe & Morris (1958), but it is classified as A0 III* by Gray & Garrison (1987) and B9.5 IV/V by Houk & Cowley (1975). Soubiran et al. (2016) give log $g = 3.42$, more consistent with a dwarf than a giant.

[7] https://irsa.ipac.caltech.edu/data/SPITZER/docs/irac/calibrationfiles/spectralresponse/

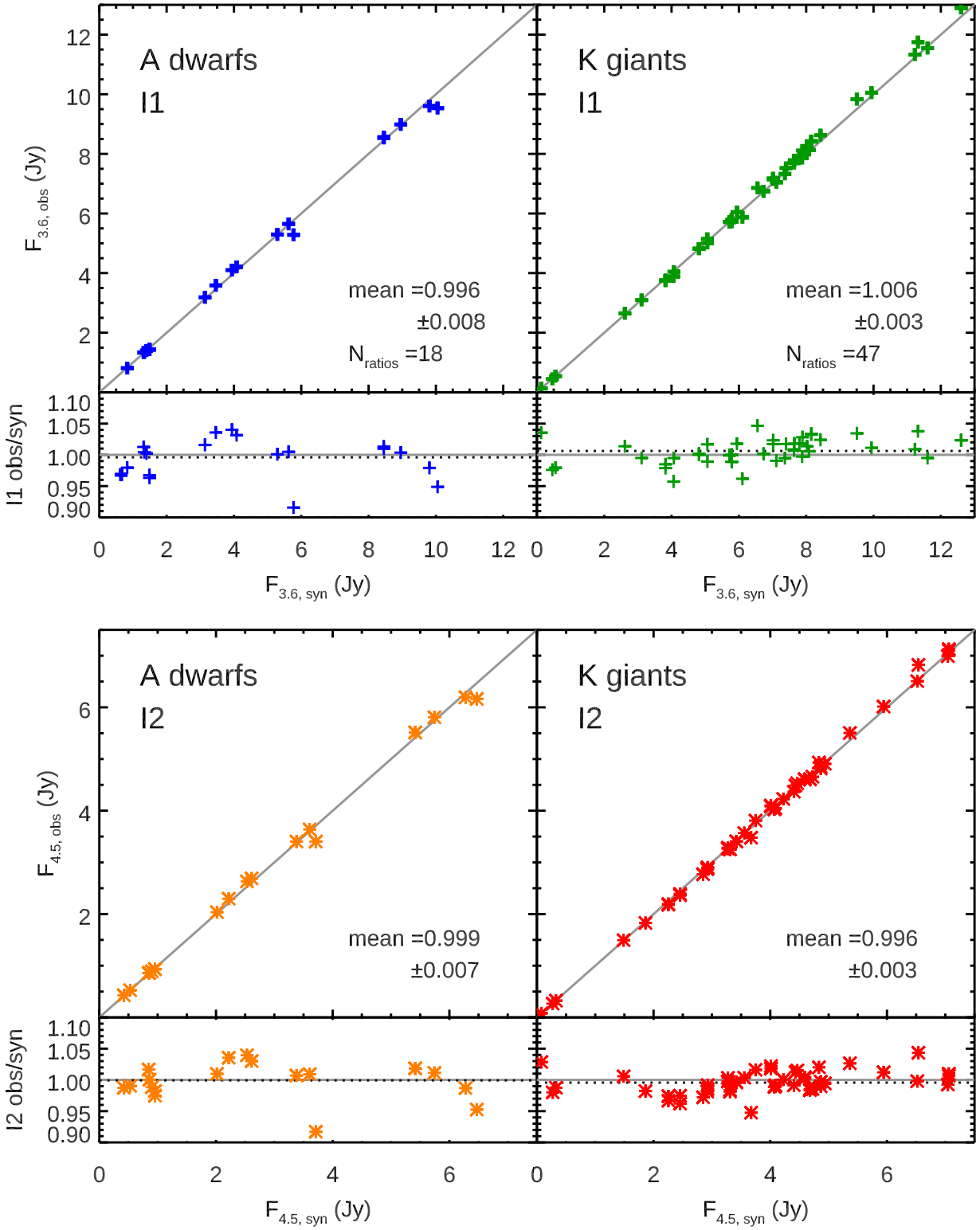

Figure 5. Observed and synthetic photometry comparison. The upper portion of each panels shows the synthetic photometry as a function of the observed photometry. The lower portions show the ratio of observed to synthetic photometry. The solid gray lines indicate equality between the two sets of photometry. (Left) The A star panels include 18 observations of 16 stars. (Right) The K stars include 47 observations of 37 stars. I1 and I2 are in the top and bottom panels, respectively. The dotted lines in ratio panels show the mean for that subset.

Figure 5 shows the results for each band, with the A dwarfs and K giants shown separately. The top section of each panel compares the IRAC flux densities to the synthetic photometry, and the lower section shows the ratios.

3.1. A Dwarfs

The 18 observations of the 16 A dwarfs show very good agreement between the observed and synthetic photometry. They have a mean ratio of observed IRAC to synthetic

Table 5
Krick et al. Photometry Comparison

Star Name	$F_{3.6}$ (Jy)		$F_{4.5}$ (Jy)	
	This work	Krick+21	This work	Krick+21
η^1 Dor	1.405 ± 0.009	1.395 ± 0.002	0.862 ± 0.007	0.887 ± 0.002
HR 5467	1.334 ± 0.012	1.335 ± 0.001	0.860 ± 0.004	0.866 ± 0.001
δ UMi	5.765 ± 0.023	5.679 ± 0.001	3.637 ± 0.023	3.658 ± 0.001
HD 163466	0.813 ± 0.009	0.816 ± 0.001	0.525 ± 0.005	0.529 ± 0.001
HD 165459[a]	0.660 ± 0.025	0.652 ± 0.001	0.421 ± 0.001	0.425 ± 0.001

Note.
[a] Flux densities of HD 165459 listed for this work are the means of the three observations and the uncertainty is the standard deviation among the three.

photometry of 0.996 ± 0.008 at 3.6 μm and 0.999 ± 0.007 at 4.5 μm. The uncertainties here are the uncertainties in the mean, i.e., the standard deviation divided by $\sqrt{N}$ where N = 18.

We can also compare our results to the recent analysis of Krick et al. (2021). They analyzed the IRAC photometry of stars which may be used for calibration of JWST, from both the cryogenic and postcryogenic portions of the Spitzer mission. Table 5 compares the photometry for the five sources we have in common. The mean ratio of our photometry to that of Krick et al. is 1.002 at 3.6 μm and 0.995 at 4.5 μm, respectively. For both wavelengths,the uncertainties in the mean are 0.003. The individual ratios are also statistically indistinguishable from unity. We conclude that our processing agrees with the results of Krick et al. (2021), which were based on a much larger set of observations taken with a wide range of observing settings.

3.2. K Giants

For the 47 observations of the 37 K giants, the mean ratios of the observed IRAC photometry to the synthetic photometry are 1.006 ± 0.003 at 3.6 μm and 0.996 ± 0.003 at 4.5 μm. The 1–2 σ deviation from unity may reflect variations in the strengths of the molecular absorption bands present in individual K giants, as has been seen previously (e.g., Heras et al. 2002; Engelke et al. 2006). As with the A dwarfs, the IRAC and IRS data agree well at both wavelengths.

4. Summary

We have presented new IRAC observations of 61 stars which were part of the IRS calibration program. The measured photometry at 3.6 and 4.5 μm was compared to synthetic photometry from stellar templates based on the IRS spectra normalized between 6 and 7 μm. For the 18 observations of the 16 A stars, the mean ratios are 0.996 ± 0.008 at 3.6 μm and 0.999 ± 0.007 at 3.6 μm and 4.5 μm, respectively. For the K stars, which had 47 observations of 37 stars, the mean ratios are 1.006 ± 0.003 and 0.996 ± 0.003 at 3.6 μm and 4.5 μm, respectively. Overall, we conclude that the IRAC and IRS calibrations agree to within 1%.

This work is based on observations made with the Spitzer Space Telescope, which is operated by the Jet Propulsion Laboratory, California Institute of Technology under NASA contract 1407. Financial support for this work was provided by NASA through NASA ADAP grant NNX17AF23G. We thank I. Sahinidis for performing the initial data quality assessment of the IRAC observations. We made use of the NASA Astrophysics Data System, IRSA's Gator service, and CDS's Simbad & Vizier services. We especially thank the referee whose vital insight into IRAC pixel phases and source positions from different extraction methods corrected our processing pipeline and significantly improved our results.

Facilities: Spitzer (IRS), Spitzer (IRAC).

Appendix
HD 165459

Table 6 gives the photometry produced by our pipeline for HD 165459 for the individual calibration observations taken by the instrument team. These used subarray mode with the 4-position large-scale Gaussian dither pattern with $t_{\rm int} = 0.4$ s. The values $F_{3.6{\rm meas}}$ and $F_{4.5{\rm meas}}$ are the means of the four positions (BCD s), weighted by σ_f, the standard deviation among the frames of a given BCD. The uncertainty reported is the weighted uncertainty.Also given are the differences between the measured value and the fiducial value from Reach et al. (2005), Δ from 6.593 mag and 6.575 mag for I1 and I2, respectively. Our pipeline gives consistently fainter values than the fiducial in both bands. We use the weighted mean of the magnitude offsets to correct the photometry in magnitude spacefor our target stars in each band.

Table 6
HD 165459 Calibration Photometry

AOR	[I1] (mag)	$F_{3.6meas}$ (Jy)	Δ from 6.593 mag (mag)	Δ from 6.593 mag (%)	[I2] (mag)	$F_{4.5meas}$ (Jy)	Δ from 6.575 mag (mag)	Δ from 6.575 mag (%)
57825280	6.625 ± 0.002	0.629 ± 0.001	0.032	−2.9	6.612 ± 0.002	0.407 ± 0.001	0.037	−3.3
57844224	6.628 ± 0.002	0.627 ± 0.001	0.035	−3.3	6.609 ± 0.002	0.408 ± 0.001	0.034	−3.0
58480128	6.626 ± 0.002	0.628 ± 0.001	0.033	−3.1	6.611 ± 0.002	0.408 ± 0.001	0.036	−3.2
58508032	6.628 ± 0.002	0.627 ± 0.001	0.035	−3.3	6.610 ± 0.002	0.408 ± 0.001	0.035	−3.2
58536448	6.629 ± 0.002	0.627 ± 0.001	0.036	−3.2	6.606 ± 0.002	0.409 ± 0.001	0.031	−2.8
58593024	6.629 ± 0.002	0.627 ± 0.001	0.036	−3.2	6.615 ± 0.002	0.406 ± 0.001	0.040	−3.6
58730496	6.629 ± 0.002	0.626 ± 0.001	0.036	−3.3	6.609 ± 0.002	0.408 ± 0.001	0.034	−3.1
58748416	6.631 ± 0.002	0.626 ± 0.001	0.038	−3.5	6.609 ± 0.002	0.408 ± 0.001	0.034	−3.1
58821888	6.632 ± 0.002	0.625 ± 0.001	0.039	−3.6	6.612 ± 0.002	0.407 ± 0.001	0.037	−3.3
58857984	6.634 ± 0.002	0.624 ± 0.001	0.041	−3.7	6.607 ± 0.002	0.409 ± 0.001	0.032	−2.9
58879232	6.628 ± 0.002	0.627 ± 0.001	0.035	−3.2	6.614 ± 0.002	0.406 ± 0.001	0.039	−3.5
58909952	6.631 ± 0.002	0.626 ± 0.001	0.038	−3.5	6.607 ± 0.002	0.409 ± 0.001	0.032	−2.9
58939392	6.627 ± 0.002	0.628 ± 0.001	0.034	−3.1	6.612 ± 0.002	0.407 ± 0.001	0.037	−3.3
58968576	6.632 ± 0.002	0.625 ± 0.001	0.039	−3.6	6.612 ± 0.002	0.407 ± 0.001	0.037	−3.4
59271168	6.631 ± 0.002	0.626 ± 0.001	0.038	−3.4	6.612 ± 0.002	0.407 ± 0.001	0.037	−3.3
59289856	6.627 ± 0.002	0.628 ± 0.001	0.034	−3.1	6.614 ± 0.002	0.407 ± 0.001	0.039	−3.4
59417856	6.628 ± 0.002	0.627 ± 0.001	0.035	−3.3	6.614 ± 0.002	0.407 ± 0.001	0.039	−3.4
59619072	6.630 ± 0.002	0.626 ± 0.001	0.037	−3.4	6.613 ± 0.002	0.407 ± 0.001	0.038	−3.4
60101888	6.629 ± 0.002	0.626 ± 0.001	0.036	−3.3	6.605 ± 0.002	0.410 ± 0.001	0.030	−2.7
60276224	6.631 ± 0.002	0.625 ± 0.001	0.038	−3.5	6.609 ± 0.002	0.408 ± 0.001	0.034	−3.0
60612608	6.631 ± 0.002	0.625 ± 0.001	0.038	−3.5	6.609 ± 0.002	0.408 ± 0.001	0.034	−3.0
60630528	6.631 ± 0.002	0.625 ± 0.001	0.038	−3.5	6.613 ± 0.002	0.407 ± 0.001	0.038	−3.4

(This table is available in its entirety in machine-readable form.)

ORCID iDs

Kathleen E. Kraemer https://orcid.org/0000-0002-2626-7155
G. C. Sloan https://orcid.org/0000-0003-4520-1044

References

Buscombe, W., & Morris, P. M. 1958, MNRAS, 118, 609
Cohen, M., Walker, R. G., Carter, B., et al. 1999, AJ, 117, 1864
Cohen, M., Walker, R. G., & Witteborn, F. C. 1992, AJ, 104, 2030
Cohen, M., Witteborn, F. C., Walker, R. G., Bregman, J. D., & Wooden, D. H. 1995, AJ, 110, 275
Cutri, R. M., Wright, E. L., Conrow, T., et al. 2013, Explanatory Supplement to the AllWISE Data Release Products
de Graauw, T., Haser, L. N., Beintema, D. A., et al. 1996, A&A, 315, L49
de Vaucouleurs, A. 1957, MNRAS, 117, 449
Engelke, C. W., Price, S. D., & Kraemer, K. E. 2006, AJ, 132, 1445
Fazio, G. G., Hora, J. L., Allen, L. E., et al. 2004, ApJS, 154, 10
Gray, R. O., & Garrison, R. F. 1987, ApJS, 65, 581
Heras, A. M., Shipman, R. F., Price, S. D., et al. 2002, A&A, 394, 539
Houck, J. R., Roellig, T. L., van Cleve, J., et al. 2004, ApJS, 154, 18
Houk, N., & Cowley, A. P. 1975, University of Michigan Catalogue of Two-dimensional Spectral Types for the HD Stars, Vol. 1 (Ann Arbor, MI: Univ. of Michigan)
Kessler, M. F., Steinz, J. A., Anderegg, M. E., et al. 1996, A&A, 315, L27
Krick, J. E., Lowrance, P., Carey, S., et al. 2021, AJ, 161, 177
Pickles, A. J. 1998, PASP, 110, 863
Reach, W. T., Megeath, S. T., Cohen, M., et al. 2005, PASP, 117, 978
Rieke, G. H., Blaylock, M., Decin, L., et al. 2008, AJ, 135, 2245
Rieke, G. H., Young, E. T., Engelbracht, C. W., et al. 2004, ApJS, 154, 25
Sloan, G. C., Herter, T. L., Charmandaris, V., et al. 2015, AJ, 149, 11
Sloan, G. C., Kraemer, K. E., Price, S. D., & Shipman, R. F. 2003, ApJS, 147, 379
Sloan, G. C., & Ludovici, D. 2012, arXiv:1212.6269
Soubiran, C., Le Campion, J.-F., Brouillet, N., & Chemin, L. 2016, A&A, 591, A118
Wright, E. L., Eisenhardt, P. R. M., Mainzer, A. K., et al. 2010, AJ, 140, 1868